CHAPTER

Turbulent Flows

8

8.1 Introduction

Turbulent flow is defined as a flow with random variation of various flow quantities such as velocity, pressure, and density. Turbulence is a property of the flow, not the property of a fluid. Despite serious progress on the topic of turbulence modeling over the last century, one has to admit that turbulence is still an unresolved problem and will remain so for a foreseeable future. In this chapter we will provide a brief overview on the numerical solution of turbulent fluid dynamics equations, based upon existing turbulence models and the characteristic-based split (CBS) scheme. We also make reference to various other works on turbulent flows and numerical modeling. Before going into such details we have summarized some important fundamental properties of turbulence in the following paragraphs. At this point it is worth noting that a turbulent flow is three-dimensional and occurs at relatively high Reynolds numbers. The turbulent flow is marked with random variation of quantities as shown in Fig. 8.1.

The Navier-Stokes equations are sufficient to resolve all turbulent scales if adequate mesh resolution is used. However, this requires extremely large computer resources. With present-day computers this is possible only for low Reynolds numbers. Until sufficiently fast computing power is available it is essential to employ Reynolds decomposition and turbulence models.

In a real turbulent flow the kinetic energy is transferred from larger scales to smaller scales. At the smallest scale the kinetic energy is transformed into internal energy; this process is called dissipation and the process of energy transfer between the scales is called "the cascade process." The smallest turbulent length scale is determined by the molecular viscosity and the rate of kinetic energy dissipation. Such a length scale is often referred to as *Kolmogorov length scale*, η [1], and given as

$$\left(\frac{\nu^3}{\varepsilon}\right)^{1/4} \tag{8.1}$$

where ν is the kinematic viscosity and ε is the average rate of dissipation of turbulent kinetic energy. Similarly Kolmogorov velocity and time scales are denoted by

$$v = (\nu\varepsilon)^{1/4} \tag{8.2}$$

Finite Element Meth Fluid Dynam 7E, Volume 3. http://dx.doi.org/10.1016/B978-1-85617-635-4.00008-X

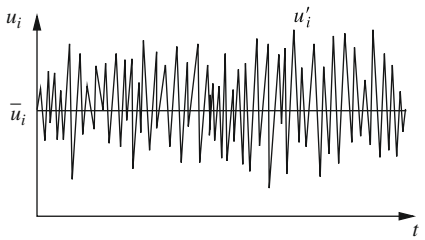

FIGURE 8.1
Random variation of velocity in a turbulent flow with respect to time.

and

$$\tau = \left(\frac{\nu}{\varepsilon}\right)^{1/2} \tag{8.3}$$

The turbulent kinetic energy dissipation rate occurring at small scales can be linked to the energy of large eddies as

$$\varepsilon = \frac{U^3}{l} \tag{8.4}$$

where U is the large eddy velocity scale and l is the large eddy length scale.

The above relations are given here to make the readers aware that the length scales and dissipation rate are closely related. The turbulence modeling procedures are developed based on these relationships.

8.1.1 Time averaging

As mentioned previously extremely high mesh resolution is required to solve down to the smallest turbulence scales. This is very expensive and presently not possible for high Reynolds number flows. It is, therefore, obvious that other alternatives are necessary to get an approximate solution. The standard procedure is to employ time-averaged Navier-Stokes equations along with a turbulence modeling approach to determine the essential time-averaged quantities, which reduces the excessive grid resolution otherwise needed. With reference to Fig. 8.1 any turbulence quantity of interest may be expressed as

$$\phi = \overline{\phi} + \phi' \tag{8.5}$$

The time-averaged quantity may be defined as

$$\overline{\phi} = \frac{1}{2T}\int_{-T}^{T} \phi(t)\, dt \tag{8.6}$$

To demonstrate time averaging we consider a one-dimensional steady state incompressible momentum equation:

$$\frac{\mathrm{d}}{\mathrm{d}x}(u^2) + \frac{1}{\rho}\frac{\mathrm{d}p}{\mathrm{d}x} - \frac{\mathrm{d}}{\mathrm{d}x}\left(\nu\frac{\mathrm{d}u}{\mathrm{d}x}\right) = 0 \tag{8.7}$$

Substituting a variation of the form of Eq. (8.5) for velocity u and pressure p into Eq. (8.7) and time averaging, we have

$$\frac{\mathrm{d}}{\mathrm{d}x}\left[\overline{(\overline{u}+u')(\overline{u}+u')}\right] + \frac{1}{\rho}\frac{\mathrm{d}}{\mathrm{d}x}\overline{(\overline{p}+p')} - \frac{\mathrm{d}}{\mathrm{d}x}\left[\nu\frac{\mathrm{d}}{\mathrm{d}x}\overline{(\overline{u}+u')}\right] = 0 \tag{8.8}$$

In the above equation the average of fluctuating components, $\overline{u'}$ and $\overline{p'}$, is equal to zero. Hence, a simplified form of the above equation may be written as

$$\frac{\mathrm{d}}{\mathrm{d}x}\left[(\overline{u}^2 + \overline{u'^2})\right] + \frac{1}{\rho}\frac{\mathrm{d}\overline{p}}{\mathrm{d}x} - \frac{\mathrm{d}}{\mathrm{d}x}\left[\nu\frac{\mathrm{d}}{\mathrm{d}x}(\overline{u})\right] = 0 \tag{8.9}$$

Rearranging and rewriting the above momentum equation in multidimensions and including the time term, we have

$$\rho\left(\frac{\partial\bar{u}_i}{\partial t} + \frac{\partial}{\partial x_j}(\bar{u}_j\bar{u}_i)\right) = -\frac{\partial\bar{p}}{\partial x_i} + \frac{\partial\bar{\tau}_{ij}}{\partial x_j} - \frac{\partial}{\partial x_j}(\rho\overline{u_i'u_i'}) \tag{8.10}$$

where

$$\bar{\tau}_{ij} = \mu\left(\frac{\partial\bar{u}_i}{\partial x_j} + \frac{\partial\bar{u}_j}{\partial x_i}\right) \tag{8.11}$$

is the time-averaged deviatoric stress and $\rho\overline{u_i'u_i'}$ is a new unknown referred to as *Reynolds stress*. A fundamental property of the Reynolds stress is the turbulent kinetic energy of a flow, κ, which is defined as

$$\kappa = \frac{1}{2}\overline{u_i'u_i'} \tag{8.12}$$

The *Boussinesq assumption* gives the Reynolds stress as

$$\bar{\tau}_{ij}{}^R = -\rho\overline{u_i'u_i'} = \mu_T\left(\frac{\partial\bar{u}_i}{\partial x_j} + \frac{\partial\bar{u}_j}{\partial x_i}\right) - \frac{2}{3}\rho\kappa\delta_{ij} \tag{8.13}$$

From Eq. (8.13) it is clear that the unknown quantity to be modeled is the turbulent dynamic viscosity $\mu_T = \rho\nu_T$. Often the last term in the above equation is dropped for simplicity.

8.1.2 Relation between κ, ε, and ν_T

The turbulent kinematic viscosity or turbulent eddy viscosity ν_T has the same dimensions as the laminar kinematic viscosity. Thus, we can express the turbulent eddy viscosity in terms of velocity and length scales of a large eddy, i.e.,

$$\nu_T = CUl \tag{8.14}$$

where C is a constant. The definitions of U and l are discussed in Section 8.1. In the above equation U may be replaced with $\sqrt{\kappa}$. With such a substitution the turbulent eddy viscosity may be determined by solving a scalar transport equation for κ and assuming an appropriate turbulent length scale l ($\kappa - l$ or one-equation models). However, a better expression for turbulent eddy viscosity may be obtained by substituting Eq. (8.4) into Eq. (8.14) as

$$\nu_T = c_\mu \frac{\kappa^2}{\varepsilon} \tag{8.15}$$

where c_μ is a constant. To employ the above equation, we need to solve two transport equations, one for κ and another for ε ($\kappa - \varepsilon$ or two-equation model). Details of many one- and two-equation models are provided in the following sections.

In the sections that follow we treat the incompressible and compressible flows separately and identify the differences. In addition to discussions on the Reynolds-averaged Navier-Stokes (RANS) models, we also provide brief summary of large eddy simulation (LES) and topics such as detached eddy simulation (DES) and monotonically integrated LES (MILES) approaches. Many useful examples are also provided to demonstrate the presented turbulent flow modeling approaches. For further details on turbulence and turbulence modeling the readers are referred to standard textbooks on this topic [2–4].

8.2 Treatment of incompressible turbulent flows

8.2.1 Reynolds-averaged Navier-Stokes

For turbulent flow computations, Reynolds-averaged Navier-Stokes equations of motion are written in conservation form as follows:

Mean-continuity

$$\frac{1}{\beta^2}\frac{\partial \bar{p}}{\partial t} + \frac{\partial(\rho \bar{u}_i)}{\partial x_i} = 0 \tag{8.16}$$

Mean-momentum

$$\rho\left(\frac{\partial \bar{u}_i}{\partial t} + \frac{\partial}{\partial x_j}(\bar{u}_j \bar{u}_k)\right) = -\frac{\partial \bar{p}}{\partial x_i} + \frac{\partial \bar{\tau}_{ij}}{\partial x_j} + \frac{\partial \bar{\tau}_{ij}^R}{\partial x_j} \tag{8.17}$$

where β is an artificial compressibility parameter, $\bar{u}_i$ are the mean velocity components, p is the pressure, ρ is the density, $\bar{\tau}_{ij}$ is the laminar shear stress tensor given by Eq. (8.11), and the Reynolds stress tensor $\bar{\tau}_{ij}^R$ is given in Eq. (8.13).

8.2.2 One-equation models

8.2.2.1 Wolfstein $\kappa - l$ model [5]

In this model the turbulent eddy viscosity is determined from a mixing length and turbulent kinetic energy as

$$\nu_T = c_\mu^{1/4} \kappa^{1/2} l_m \tag{8.18}$$

where c_μ is a constant equal to 0.09, κ is the turbulent kinetic energy, and l_m is a mixing length. The mixing length l_m is related to the length scale of turbulence L as

$$l_m = \left(\frac{c_\mu'^3}{C_D} \right)^{1/4} L \tag{8.19}$$

where C_D and c_μ' are constants.

The transport equation for turbulent kinetic energy κ is

$$\frac{\partial \kappa}{\partial t} + \frac{\partial}{\partial x_i}(\bar{u}_i \kappa) = \frac{\partial}{\partial x_i}\left(\nu + \frac{\nu_T}{\sigma_\kappa} \right) \frac{\partial \kappa}{\partial x_i} + \frac{\bar{\tau}_{ij}^R}{\rho} \frac{\partial \bar{u}_i}{\partial x_j} - \varepsilon \tag{8.20}$$

where σ_κ is the diffusion Prandtl number for turbulent kinetic energy. The dissipation, ε, is modeled as

$$\varepsilon = C_D \frac{\kappa^{3/2}}{L} \tag{8.21}$$

Near solid walls, the Reynolds number tends to zero and the highest mean velocity gradient occurs at the solid boundary. Thus, the one-equation model has to be used in conjunction with empirical wall functions, i.e., ν_T is multiplied by damping function $f_\mu = 1 - e^{-0.160 R_\kappa}$ and ε is divided by $f_b = 1 - e^{-0.263 R_\kappa}$, where $R_\kappa = \sqrt{\kappa} y / \nu$. Here y is the shortest distance to a nearest wall. The constants are $\sigma_k = 1$ and $C_D = 1.0$.

8.2.2.2 Spalart-Allmaras (SA) model [6]

The Spalart-Allmaras (SA) model was first introduced for aerospace applications and then adopted for incompressible flow calculations. This is another one-equation model that employs a single scalar equation and several constants to model turbulence. The scalar transport equation used by this model is

$$\frac{\partial \hat{\nu}}{\partial t} + \frac{\partial (u_j \hat{\nu})}{\partial x_j} = c_{b1} \hat{S} \hat{\nu} + \frac{1}{\sigma} \left[\frac{\partial}{\partial x_i}(\nu + \hat{\nu}) \frac{\partial \hat{\nu}}{\partial x_i} + c_{b2} \left(\frac{\partial \hat{\nu}}{\partial x_i} \right)^2 \right] - c_{w1} f_w \left[\frac{\hat{\nu}}{y} \right]^2 \tag{8.22}$$

where

$$\hat{S} = S + (\hat{\nu} / k^2 y^2) f_{v2} \tag{8.23}$$

$$f_{v2} = 1 - X/(1 + X f_{v1}) \tag{8.24}$$

In Eq. (8.23), S is the magnitude of vorticity and y is the shortest distance from a node to the nearest solid wall. The eddy viscosity is calculated as

$$\nu_T = \hat{\nu} f_{v1} \tag{8.25}$$

where

$$f_{v1} = X^3/(X^3 + c_{v1}^3) \tag{8.26}$$

and

$$X = \hat{\nu}/\nu \tag{8.27}$$

The parameter f_w is given as

$$f_w = g\left[\frac{1 + c_{w3}^6}{g^6 + c_{w3}^3}\right]^{1/6} \tag{8.28}$$

where

$$g = r + c_{w2}(r^6 - r) \tag{8.29}$$

and

$$r = \frac{\hat{\nu}}{\hat{S}k^2y^2} \tag{8.30}$$

The constants are $c_{b1} = 0.1355$, $\sigma = 2/3$, $c_{b2} = 0.622$, $k = 0.41$, $c_{w1} = c_{b1}/k^2 + (1 + c_{b2})/\sigma$, $c_{w2} = 0.3$, $c_{w3} = 2$, and $c_{v1} = 7.1$.

8.2.3 Two-equation models

8.2.3.1 The standard $\kappa - \varepsilon$ model

In this model, the transport equation for κ is the same as that in the one-equation model of Section 8.2.2.1. The second transport equation for calculating the turbulence energy dissipation rate ε is

$$\frac{\partial \varepsilon}{\partial t} + \frac{\partial}{\partial x_i}(\bar{u}_i\varepsilon) = \frac{\partial}{\partial x_i}\left(\nu + \frac{\nu_T}{\sigma_\varepsilon}\right)\frac{\partial \varepsilon}{\partial x_i} + C_{\varepsilon 1}\frac{\varepsilon}{\kappa}\frac{\bar{\tau}_{ij}^R}{\rho}\frac{\partial \bar{u}_i}{\partial x_j} - C_{\varepsilon 2}\frac{\varepsilon^2}{\kappa} \tag{8.31}$$

where $C_{\varepsilon 1} = 1.44$, $C_{\varepsilon 2} = 1.92$, and σ_ε is the diffusion Prandtl number for isotropic turbulence energy dissipation rate and equal to 1.3. These constants are proposed by Jones and Launder [7].

In addition, ν_T is evaluated by

$$\nu_T = C_\mu \frac{\kappa^2}{\varepsilon} \tag{8.32}$$

For near-wall treatments, modifications to the source terms of ε equation are needed in the near-wall region. Multiplying the coefficients c_μ, $C_{\varepsilon 1}$, and $C_{\varepsilon 2}$ by the

turbulence damping functions f_μ, $f_{\varepsilon 1}$, and $f_{\varepsilon 2}$, appropriate low Reynolds number status near the walls is achieved. Numerous wall damping functions have been proposed. The ones suggested by Lam and Bremhorst [8] for steady flows are

$$f_\mu = (1 - e^{-0.0165 R_\kappa})^2 \left(1 + \frac{20.5}{R_t}\right) \tag{8.33a}$$

$$f_{\varepsilon 1} = 1 + \left(\frac{0.05}{f_\mu}\right)^3 \tag{8.33b}$$

and

$$f_{\varepsilon 2} = 1 - e^{-R_t^2} \tag{8.33c}$$

where $R_t = \kappa^2/\nu\varepsilon$. The damping functions of Fan et al. [9] are

$$f_\mu = 0.4 \frac{f_w}{\sqrt{R_t}} \left(1 - 0.4 \frac{f_w}{\sqrt{R_t}}\right) \left[1 - \exp\left(-\frac{R_y}{42.63}\right)\right]^3 \tag{8.34}$$

where

$$\begin{aligned} f_w &= 1 - \exp\left\{-\frac{\sqrt{R_y}}{2.30} + \left(\frac{\sqrt{R_y}}{2.30} - \frac{R_y}{8.89}\right)\left[1 - \exp\left(-\frac{R_y}{20}\right)\right]^3\right\} \\ f_{\varepsilon 2} &= \left\{1 - \frac{0.4}{0.8} \exp\left[-\left(\frac{R_t}{6}\right)^2\right]\right\} f_w^2 \end{aligned} \tag{8.35}$$

and $f_{\varepsilon 1} = 1$. The constants are $c_\mu = 0.09$, $\sigma_k = 1.0$, $\sigma_\varepsilon = 1.3$, $C_{\varepsilon 1} = 1.4$, and $C_{\varepsilon 2} = 1.8$.

8.2.4 Nondimensional form of the governing equations

The turbulent flow solution is obtained by solving Eqs. (8.16) and (8.17) with appropriate boundary conditions along with one of the turbulence models. The following nondimensional scales may be used in the calculations:

$$\begin{aligned} \bar{u_i}^* &= \frac{\bar{u_i}}{u_\infty}, \quad x_i^* = \frac{x_i}{D}, \quad \bar{p}^* = \frac{\bar{p}}{\rho_\infty u_\infty^2}, \quad t^* = \frac{t u_\infty}{D} \\ \kappa^* &= \frac{\kappa}{u_\infty^2}, \quad \varepsilon^* = \frac{\varepsilon D}{u_\infty^3}, \quad \nu_T^* = \frac{\nu_T}{\nu_\infty}, \quad \hat{\nu}^* = \frac{\hat{\nu}}{\nu_\infty} \end{aligned} \tag{8.36}$$

where D is a characteristic length and the subscript ∞ indicates a reference value. Substituting the nondimensional scales into Eqs. (8.16) and (8.17), and dropping asterisks leads to

$$\frac{1}{\beta^2}\frac{\partial(\bar{p})}{\partial t} + \frac{\partial(\rho \bar{u_i})}{\partial x_i} = 0 \tag{8.37a}$$

$$\frac{\partial \bar{u}_i}{\partial t} + \frac{\partial}{\partial x_j}(\bar{u}_j \bar{u}_i) = -\frac{\partial \bar{p}}{\partial x_i} + \frac{\partial(\bar{\tau}_{ij} + \bar{\tau}_{ij}^R)}{\partial x_j} \tag{8.37b}$$

and

$$\bar{\tau}_{ij} + \bar{\tau}_{ij}^R = \frac{(1.0 + \nu_T)}{Re}\left(\frac{\partial \bar{u}_i}{\partial x_j} + \frac{\partial \bar{u}_j}{\partial x_i}\right) \tag{8.37c}$$

The Reynolds number, Re, in the above equation is defined as

$$Re = \frac{\bar{u}_\infty D}{\nu_\infty} \tag{8.38}$$

The viscosity, ν, is assumed to be constant and equal to ν_∞ in the above equations. Note that the turbulent kinetic energy term is dropped from Eq. (8.13) to arrive at Eq. (8.37c). The nondimensional form of the turbulence transport equations are given below

8.2.4.1 $\kappa - l$ model

The nondimensional form of the κ equation is

$$\frac{\partial \kappa}{\partial t} + \frac{\partial}{\partial x_i}(\bar{u}_i \kappa) = \frac{1}{Re}\frac{\partial}{\partial x_i}\left(1 + \frac{\nu_T}{\sigma_\kappa}\right)\frac{\partial \kappa}{\partial x_i} + \bar{\tau}_{ij}^R \frac{\partial \bar{u}_i}{\partial x_j} - \varepsilon \tag{8.39}$$

The mixing length and the turbulence length scales are normalized using the characteristic length D. In this study we assume $L = D$. The nondimensional form of R_k is $\sqrt{\kappa} y Re$.

8.2.4.2 Spalart-Allmaras model

The nondimensional form of the transport equation is

$$\frac{\partial \hat{\nu}}{\partial t} + \frac{\partial(\bar{u}_j \hat{\nu})}{\partial x_j} = c_{b1}\hat{S}\hat{\nu} + \frac{1}{Re\sigma}\left[\frac{\partial}{\partial x_i}(1 + \hat{\nu})\frac{\partial \hat{\nu}}{\partial x_i} + c_{b2}\left(\frac{\partial \hat{\nu}}{\partial x_i}\right)^2\right] - \frac{c_{w1} f_w}{Re}\left[\frac{\hat{\nu}}{y}\right]^2 \tag{8.40}$$

where

$$\hat{S} = S + \frac{1}{Re}(\hat{\nu}/k^2 y^2) f_{v2} \tag{8.41}$$

and

$$r = \frac{1}{Re}\frac{\hat{\nu}}{\hat{S}k^2 y^2} \tag{8.42}$$

The structures of all the remaining parameters are unchanged.

8.2.4.3 $\kappa - \varepsilon$ model

The κ equation is identical to that of the one-equation model and the dissipation equation is given as

$$\frac{\partial \varepsilon}{\partial t} + \frac{\partial}{\partial x_i}(\bar{u}_i \varepsilon) = \frac{1}{Re}\frac{\partial}{\partial x_i}\left(1 + \frac{\nu_T}{\sigma_\varepsilon}\right)\frac{\partial \varepsilon}{\partial x_i} + C_{\varepsilon 1}\frac{\varepsilon}{\kappa}\bar{\tau}_{ij}^R\frac{\partial \bar{u}_i}{\partial x_j} - C_{\varepsilon 2}\frac{\varepsilon^2}{\kappa} \tag{8.43}$$

The parameter R_t in its nondimensional form is $\kappa^2 Re/\varepsilon$.

8.2.5 Shortest distance to a solid wall

In all the turbulence models described above, distance from a node to the nearest wall is essential. For meshes with a small number of nodes it is a matter of checking the number of solid wall nodes against the total number of nodes in a mesh. However, such a procedure will consume a significant part of the computational time if the number of nodes is in the hundreds of thousands. Nowadays, it is common to solve flow equations over several million number of nodes. Hence, we need to have a faster and reliable wall distance calculation procedure in place.

The wall distance calculation may be accelerated by creating linelets emanating from solid wall nodes as discussed in Refs. [10,11]. This method works by allocating all nonwall nodes to a linelet and then finding a short distance to the wall. This method was proved to reduce computing time to calculate wall distance. In time-dependent flow problems which involve moving solid walls, the standard procedures of calculating the wall distances will again be expensive. In recent years, differential equation–based wall distance calculation procedures have been developed to reduce the cost of repeated wall distance computation [12–14]. One of the simplest models used to calculate shortest distance is the one based on the numerical solution of the Eikonal equation:

$$\frac{\partial \phi}{\partial t} + \left(\frac{\partial \phi}{\partial x_i}\right)^2 = 1 \tag{8.44}$$

This is a convection equation and any of the stable methods discussed in Chapter 2 may be used to solve for shortest distance to a solid wall ϕ as shown in the following example.

Example 8.1. Shortest distance to walls inside a cube

The structured and unstructured meshes of a cube of unit size are shown in Fig. 8.2. All the six surfaces of the cube are assumed to be solid walls. The exact solution is obtained using a standard search procedure of looping over the number of tetrahedron elements and surface faces. For the structured mesh, a node is placed exactly at the center of the domain to give the shortest distance to the wall of 0.5. Since a nodal position at the center is not guaranteed in an unstructured mesh, the maximum shortest distance to the nearest wall may not be 0.5.

Figure 8.3 compares the solutions obtained by the standard search procedure and the numerical solution to the Eikonal equation using both the meshes of Fig. 8.2. As seen the analytical and numerical results obtained are almost identical [14].

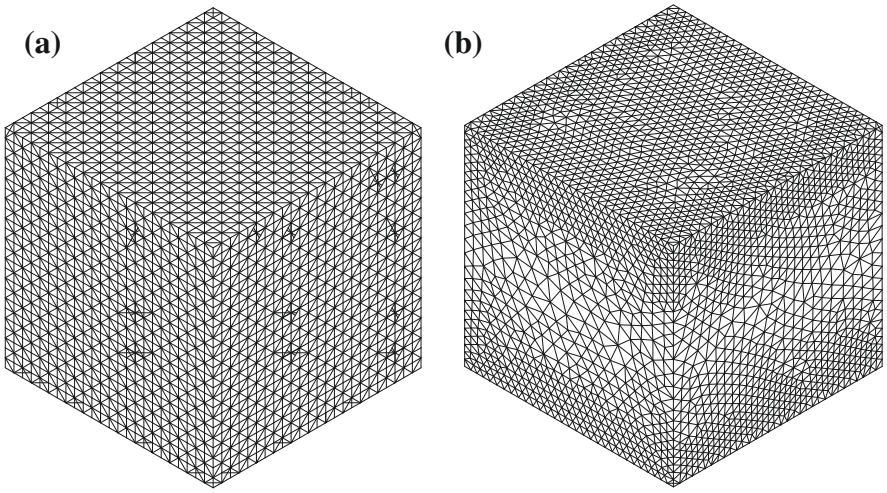

FIGURE 8.2
(a) Structured mesh S1 (nodes: 15,625; elements: 69,120); (b) unstructured mesh U1 (nodes: 23,597; elements: 127,692).

8.2.6 Solution procedure for turbulent flow equations

It is evident from the RANS equations discussed above that the governing turbulent flow equations take the form of standard fluid dynamics equations discussed in the previous chapters. However, we have additional scalar transport equation(s) that need to be solved in conjunction with the RANS equations. We therefore recommend the CBS scheme along with any valid procedure for solving the convection-diffusion equation from Chapter 2 for the solution of scalar turbulence transport equations.

The transient solutions may be obtained via an artificial compressibility scheme using a dual time-stepping algorithm [15]. Alternatively a semi- or quasi-implicit form of the scheme may be employed to obtain unsteady state solutions. Unsteady state RANS solutions are often referred to as URANS solutions [15–20].

Example 8.2. Turbulent flow in a rectangular channel

Often structured meshes are preferred for turbulent flow calculations. Since structured meshes give the best solution, we recommend structured meshes or meshes with structured layers close to the wall wherever possible. However, if unstructured meshes are employed it may be important to assess their applicability. In order to estimate the applicability of unstructured meshes we provide a comparison between the structured and unstructured mesh results for flow through a rectangular channel at a moderate Reynolds number of 12,300. Figures 8.4 and 8.5 show the results. The first node of the structured mesh was placed at a distance of 0.005 and the unstructured mesh was placed roughly around 0.01. As seen the logarithmic representation of time-averaged velocity variation is close to the experimental data of Laufer [21]. The small difference between the structured and unstructured meshes is attributed to the slightly larger

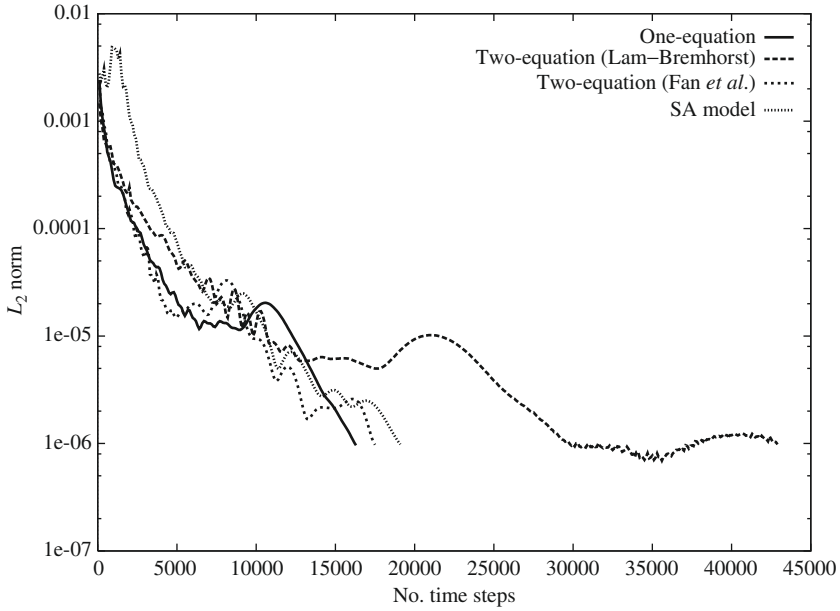

FIGURE 8.3

Wall distance contours at a central section in the x_1 direction (uniformly structured mesh S1). Comparison between search procedure and implicit GMRES scheme. (a) Simple search procedure (structured mesh): $\phi_{min} = 0.0, \phi_{max} = 0.5000$; (b) Eikonal equation (structured mesh): $\phi_{min} = 0.0, \phi_{max} = 0.5000$; (c) simple search procedure (unstructured mesh): $\phi_{min} = 0.0, \phi_{max} = 0.4923$; (d) Eikonal equation (unstructured mesh): $\phi_{min} = 0.0, \phi_{max} = 0.4887$.

elements of the unstructured mesh used close to the wall. The point we are trying to prove here is that the turbulence model and the artificial compressibility–based CBS schemes together can predict the time-averaged turbulence quantities satisfactorily. In several ways these results allow us to present the unstructured mesh results with confidence. We also show the comparison of fully developed velocity profiles with the experimental data of Laufer [21] in Fig. 8.5a. As seen the agreement between the numerical and experimental data is excellent. Figure 8.5b shows the convergence histories of structured and unstructured meshes to steady state. As seen the convergence is rapid and it took only about 5000 time steps to reach an L_2 norm velocity residual of 10^{-5}. We use local time steps to accelerate the solution to steady state.

Example 8.3. Turbulent flow past a backward facing step

A standard test case commonly employed for testing turbulent incompressible flow models at a moderate Reynolds number is the recirculating flow past a backward facing step. Unlike the channel flow, here the model has to handle the recirculation region immediately downstream of the step. The nonequilibrium turbulent flow conditions in the recirculation region make most of the one-equation turbulence models inadequate.

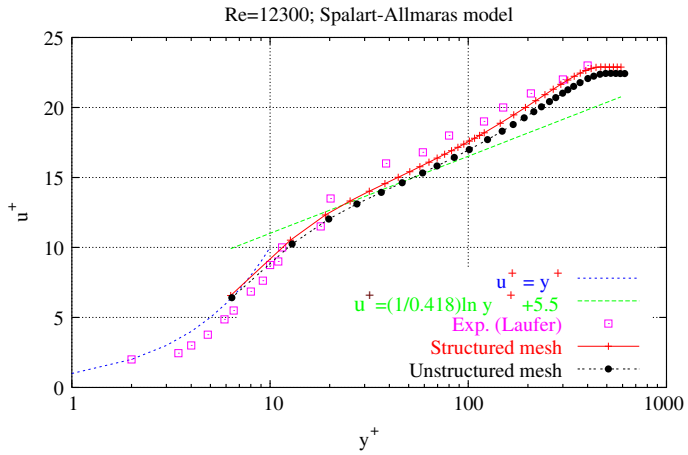

FIGURE 8.4

Turbulent incompressible flow through a rectangular channel using the Spalart-Allmaras model at $Re = 12{,}300$. Logarithmic representation of time-averaged velocity profile. (Note: $u^+ = u/u_\tau$ with $u_\tau = \sqrt{\tau_W/\rho}$ being the friction velocity; $y^+ = yu_\tau/\nu$ with y being the shortest distance to the wall.)

The definition of the problem is shown in Fig. 8.6. The characteristic dimension of the problem is the step height (L). All other dimensions are defined with respect to this. The inlet is located at a distance of four times the step height upstream of the step. The inlet channel height is $2L$. The total length of the channel is $40L$.

The inlet velocity profile is obtained from measurements reported by Denham et al. [22]. No-slip conditions apply on the solid walls. For the one-equation and two-equation models the inlet κ and ε profiles were obtained by solving a channel flow problem. For the SA model, a fixed value of 0.05 for the turbulent scalar variable at the inlet was prescribed. On the walls κ was assumed to be equal to zero. The wall conditions for ε are

$$\varepsilon = \frac{2}{Re}\left(\frac{\mathrm{d}\kappa^{1/2}}{\mathrm{d}y}\right)^2 \tag{8.45}$$

as discussed in Ref. [23]. The scalar variable of the SA model was also assumed to be zero on the walls.

Figure 8.7 shows the comparison of velocity profiles against the experimental data of Denham et al. [22]. It is obvious that the one-equation model failed to predict the recirculation region accurately. The SA model and the two-equation models on the other hand predict the recirculation better than the one-equation model. Among the SA and two-equation models, the former seems to predict the recirculation more accurately.

Both structured and unstructured meshes were employed in the calculation. Figures 8.8 and 8.9 show the SA model solutions on structured and unstructured

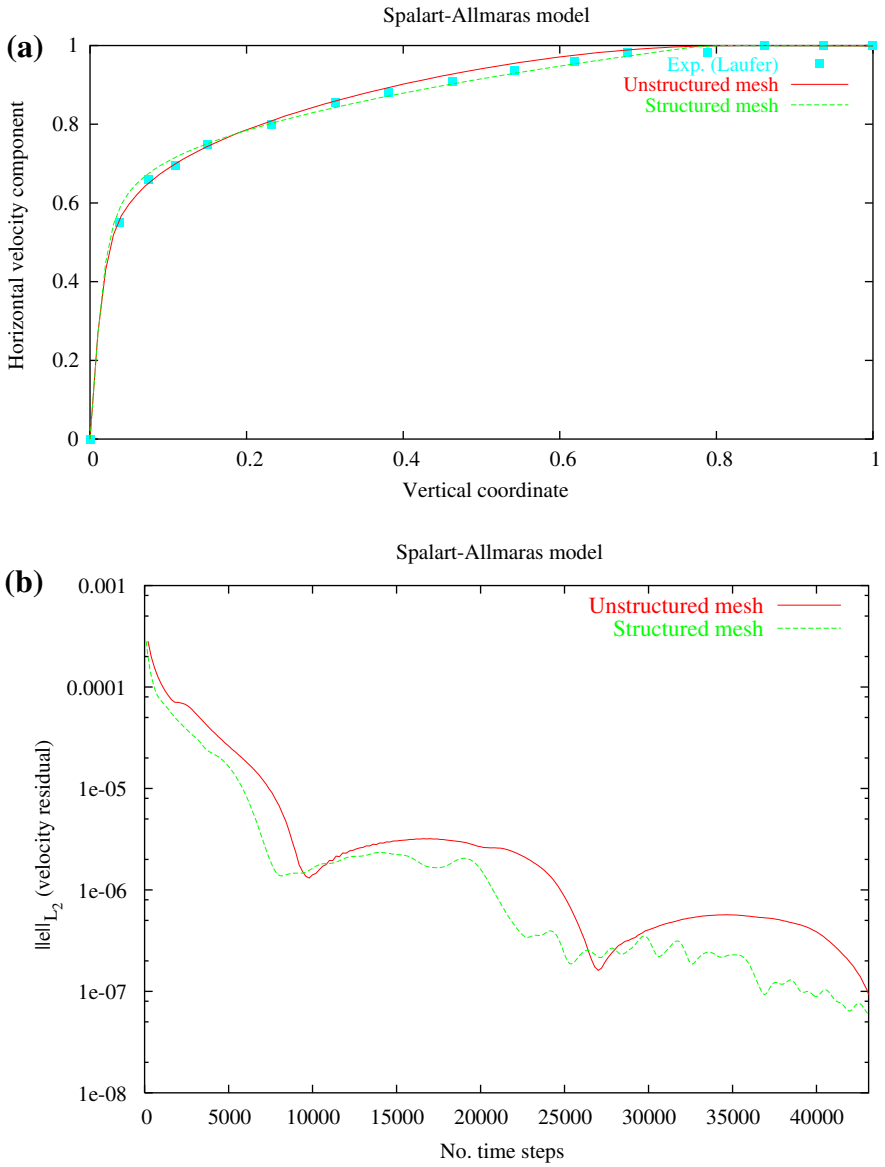

FIGURE 8.5

Turbulent incompressible flow in a rectangular channel using the Spalart-Allmaras model at $Re = 12{,}300$. (a) Comparison of fully developed velocity profiles; (b) convergence to the steady state.

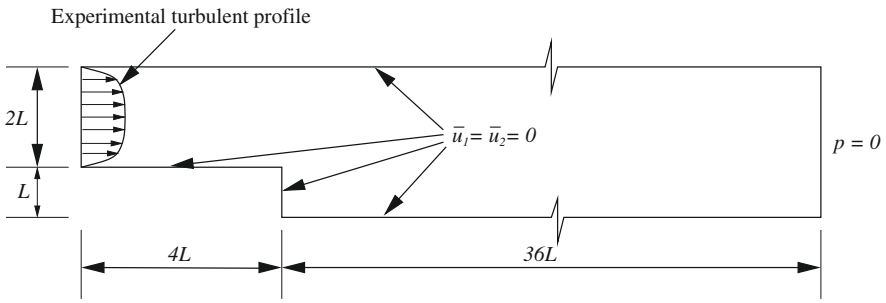

FIGURE 8.6
Turbulent flow past a two-dimensional backward facing step. Problem definition.

meshes respectively. The qualitative difference between the two results is almost nil. The quantitative difference between the two solutions was also found to be negligibly small.

Example 8.4. Unsteady turbulent flow past a circular cylinder

The example considered is the standard test case of transient turbulent incompressible flow past a circular cylinder at a Reynolds number of 10,000.

The domain consists of a circular cylinder placed at a distance of $4D$ from the inlet, where D is the diameter of the cylinder. The distance from the center of the cylinder to the top and bottom sides is equal to $4D$. The exit of the domain is placed at a distance of $12D$ from the center of the cylinder (Fig. 8.10). The finite element mesh used is shown in Fig. 8.10. The mesh in the vicinity of the cylinder and along the wake region is refined with structured layers in the vicinity of the cylinder surface to capture the transient feature of the problem.

Uniform velocity conditions were assumed at the inlet. The turbulent scalar variable was assumed to be equal to 0.05 at the inlet for the SA model. On the top and bottom sides slip conditions were assumed and no turbulence quantity was prescribed. On the cylinder walls no-slip conditions are assumed and the turbulent scalar variable of the SA model was assumed to be zero.

Dual time stepping was employed in this problem. A true transient term was added to both Step 3 of the scheme as discussed in Chapter 3 and to the turbulence transport equations. The pseudo time step used within each real time step is local and varies between the nodes depending on the local flow field and mesh size. The L_2 norm of velocity residual was reduced to less than 10^{-6} within every real time step in order to make sure that local steady state is achieved within each real time step.

Snapshots of different variables are shown in Fig. 8.11. These figures show that the vortex shedding is present (SA model).

Figure 8.12 shows temporal drag and lift coefficients when using the SA model. Periodic flow and vortex shedding are clearly evident from the graphs. The average experimental value of drag coefficient is around 1.12 and the Strouhal number is

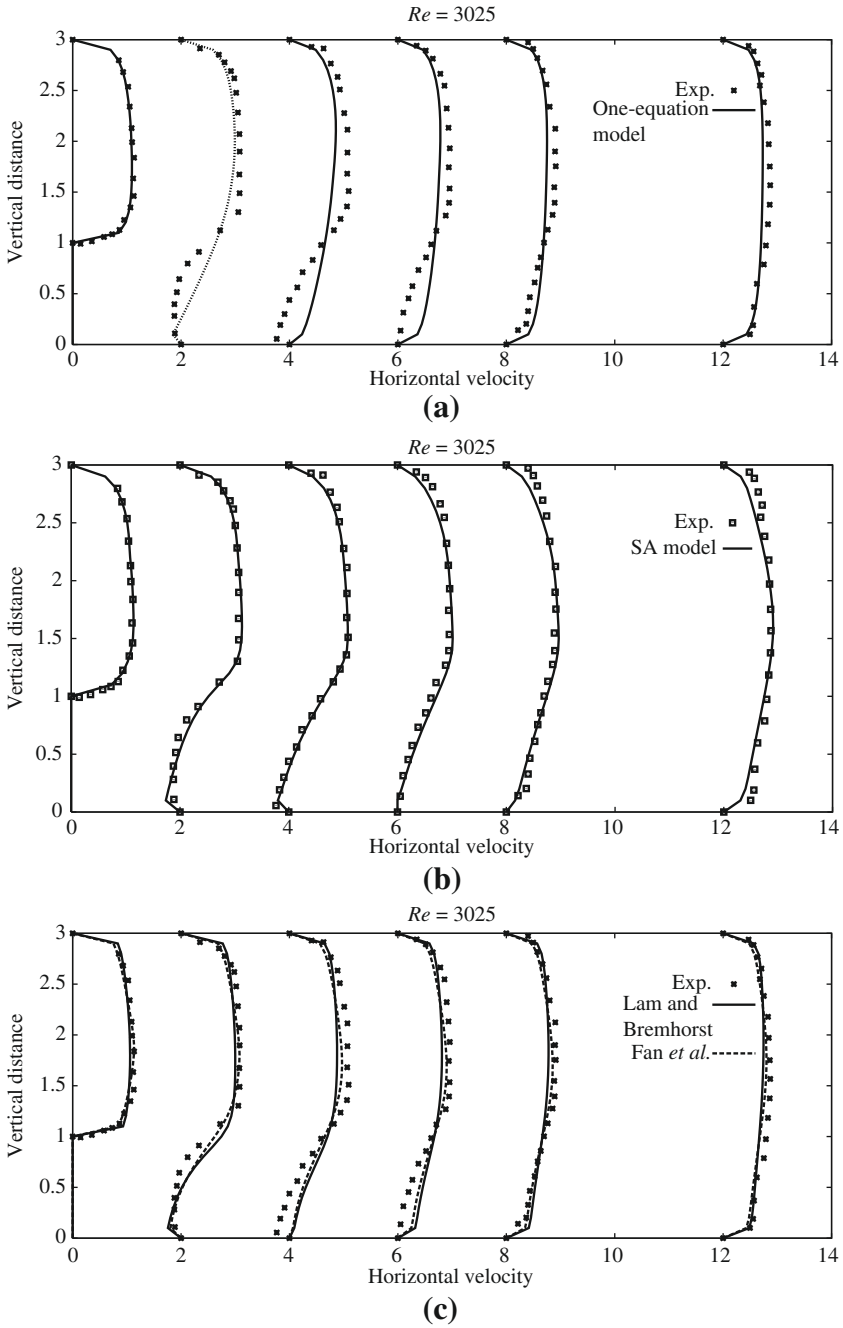

FIGURE 8.7

Incompressible turbulent flow past a backward facing step. Velocity profiles at various downstream sections at $Re = 3025$: (a) one-equation model; (b) SA model; (c) two-equation model.

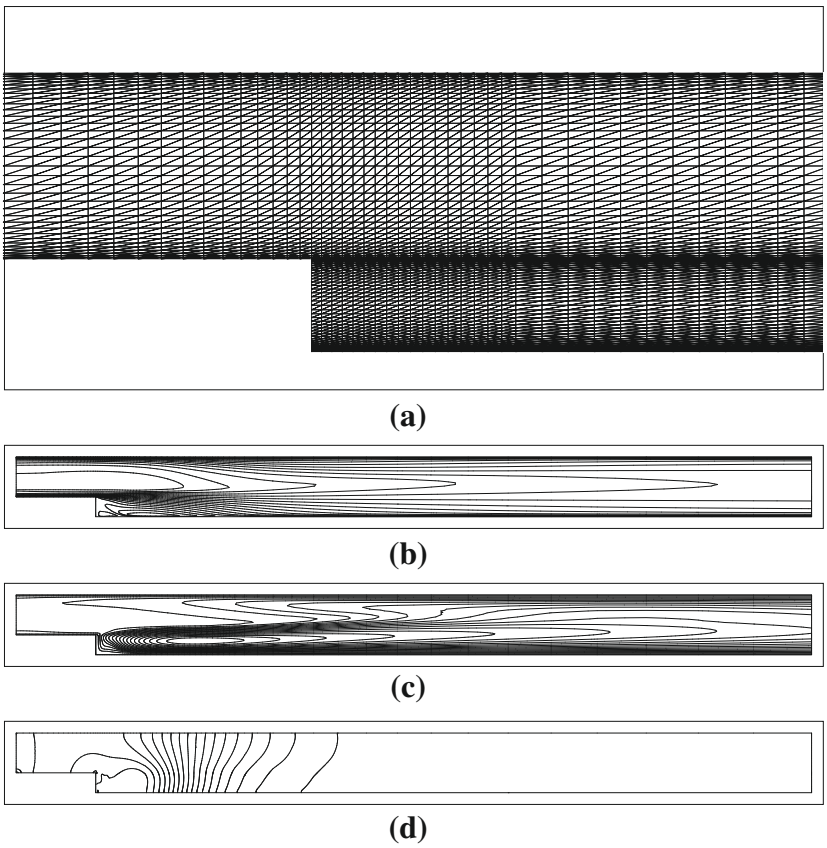

FIGURE 8.8
Incompressible turbulent flow past a backward facing step (a) Structured mesh (elements: 8092, nodes: 4183), (b) velocity contours, (c) $\hat{\nu}$ contours, and (d) pressure contours at $Re = 3015$ using the SA model.

around 0.2 [24]. The time-averaged coefficient of pressure distribution is shown in Fig. 8.13.

8.3 Treatment of compressible flows

The conservation equations for compressible flows may be rewritten from Chapters 1 and 2.

Mass conservation

$$\frac{\partial \rho}{\partial t} = \frac{1}{c^2}\frac{\partial p}{\partial t} = -\frac{\partial U_i}{\partial x_i} \tag{8.46}$$

where c is the speed of sound and depends on E, p, and ρ.

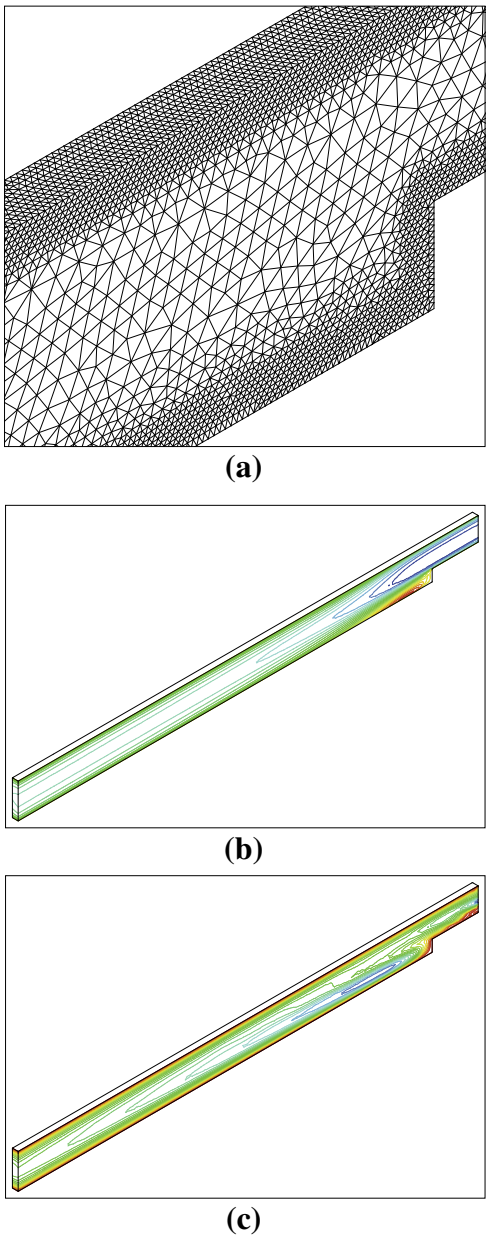

FIGURE 8.9

Incompressible turbulent flow past a backward facing step (a) Unstructured mesh (elements: 47,359, nodes: 24,336), (b) velocity contours, and (c) $\hat{\nu}$ contours at $Re = 3025$ using the SA model.

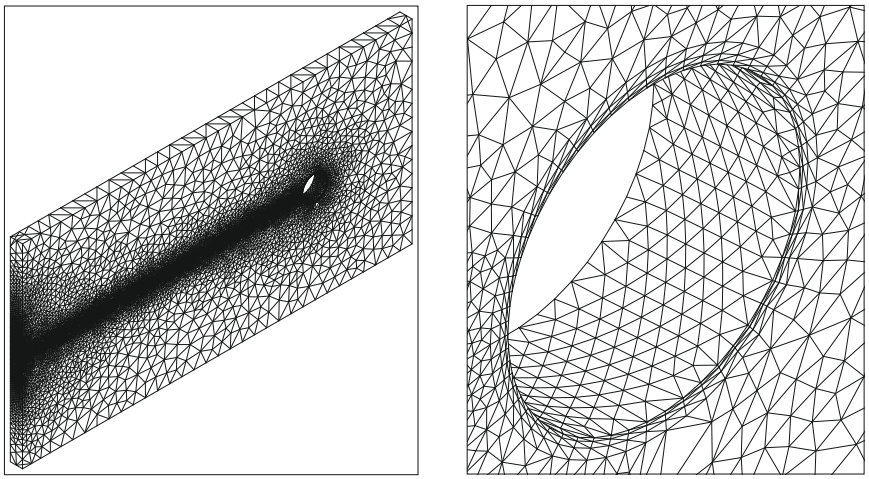

FIGURE 8.10
Incompressible turbulent flow past a circular cylinder. Finite element mesh: (a) overall mesh; (b) close-up of the cylinder.

Momentum conservation

$$\frac{\partial U_i}{\partial t} = -\frac{\partial}{\partial x_j}(u_j U_i) + \frac{\partial \tau_{ij}}{\partial x_j} - \frac{\partial p}{\partial x_i} + \rho g_i \tag{8.47}$$

Energy conservation

$$\frac{\partial(\rho E)}{\partial t} = -\frac{\partial}{\partial x_i}(u_i \rho E) + \frac{\partial}{\partial x_i}\left(k\frac{\partial T}{\partial x_i}\right) - \frac{\partial}{\partial x_i}(u_i p) + \frac{\partial}{\partial x_i}(\tau_{ij} u_j) + \rho g_i u_i \tag{8.48}$$

In all of the above u_i are the velocity components, ρ is the density, E is the specific energy, p is the pressure, T is the absolute temperature, ρg_i represents body forces and other source terms, k is the thermal conductivity, and τ_{ij} are the deviatoric stress components given by [Eq. (1.11b)]

$$\tau_{ij} = \mu\left(\frac{\partial u_i}{\partial x_j} + \frac{\partial u_j}{\partial x_i} - \tfrac{2}{3}\delta_{ij}\frac{\partial u_k}{\partial x_k}\right) \tag{8.49}$$

In general, the dynamic viscosity μ in the above equation is a function of temperature, $\mu(T)$, and appropriate relations will be used if necessary (see Chapter 7).

8.3.1 Mass-weighted (Favre) time averaging

Conventional time averaging discussed in Section 8.1.1 introduces additional terms in compressible flows and needs additional equations to close the system. Thus, in compressible flow calculations it is often useful to introduce mass-weighted averaging.

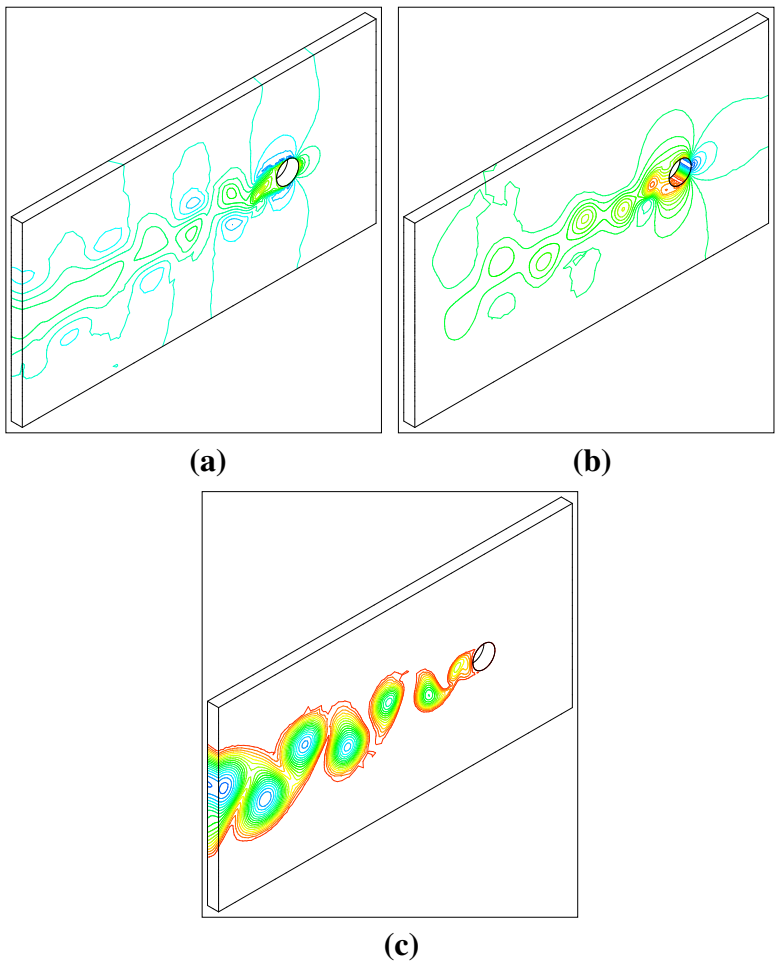

FIGURE 8.11
Incompressible turbulent flow past a circular cylinder. Snapshots of variables at $Re = 10{,}000$ using the SA model: (a) u_1 contours; (b) p contours; (c) ν_T contours.

In such a procedure, a mass-weighted average velocity is given as

$$\tilde{u_i} = \frac{\overline{\rho u_i}}{\overline{\rho}} \tag{8.50}$$

where the overline in the above equation indicates a standard time-averaged quantity. Here, the time-dependent velocity may be written as

$$u_i = \tilde{u_i} + u_i'' \tag{8.51}$$

The above equation has a similar form as standard time averaging relation (8.5). However, in the above equation the mass-weighted averaging term $\tilde{u_i}$ replaces the

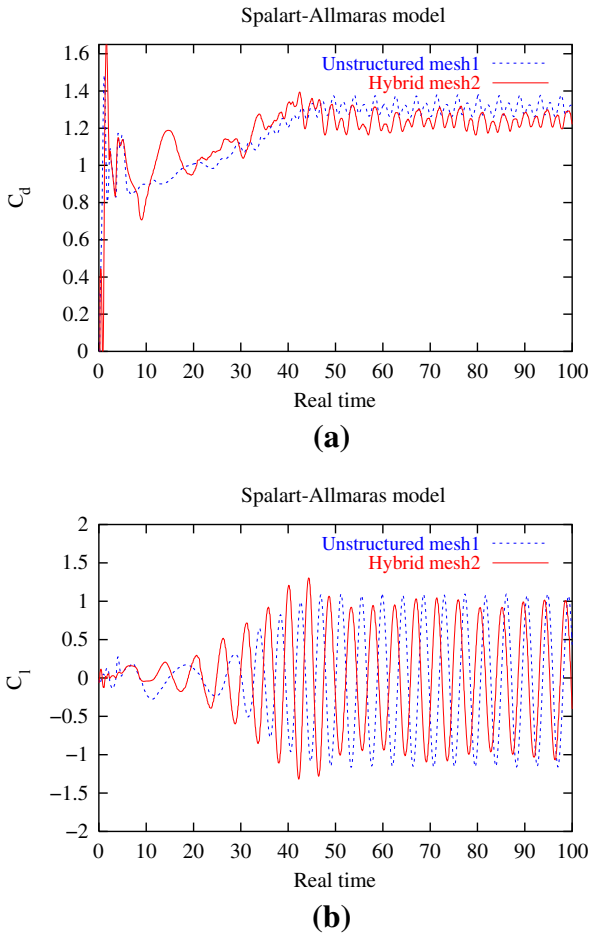

FIGURE 8.12

Incompressible turbulent flow past a circular cylinder. (a) Drag and (b) lift coefficient distributions with respect to real time at $Re = 10{,}000$ using the SA model.

conventional time averaging term $\bar{u_i}$. Now employing the mass-weighted velocity and standard time averaging for ρ and p we get the conservation of mass and momentum equations as

$$\frac{\partial \bar{\rho}}{\partial t} + \frac{\partial}{\partial x_i}(\bar{\rho}\tilde{u_i}) = 0 \tag{8.52}$$

and

$$\frac{\partial}{\partial t}(\bar{\rho}\tilde{u_i}) + \frac{\partial}{\partial x_j}(\bar{\rho}\tilde{u_i}\tilde{u_j}) = -\frac{\partial \bar{p}}{\partial x_i} + \frac{\partial}{\partial x_j}(\bar{\tau_{ij}} - \overline{\rho u_i'' u_j''}) \tag{8.53}$$

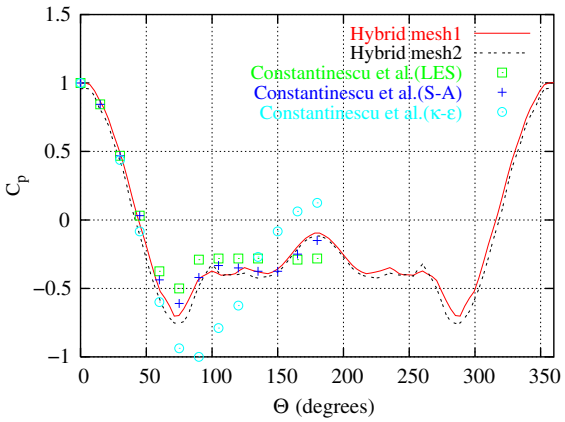

FIGURE 8.13

Incompressible turbulent flow past a circular cylinder. Time-averaged coefficient of pressure at $Re = 10{,}000$ using the SA model. Data for comparison from Ref. [20].

It should be noted here that in standard mass averaging $\overline{u_i'} = 0$ and $\overline{\rho u_i'} \neq 0$ and in mass-weighted averaging $\overline{u_i''} \neq 0$ and $\overline{\rho u_i''} = 0$. In Eq. (8.53) $\overline{\rho u_i'' u_j''}$ are the Reynolds stresses. In a similar fashion the mass-weighted averaging for energy gives

$$\frac{\partial(\overline{\rho}\tilde{E})}{\partial t} = -\frac{\partial}{\partial x_i}(\overline{\rho}\tilde{u}_i\tilde{E}) + \frac{\partial}{\partial x_i}\left(k\frac{\partial \overline{T}}{\partial x_i} - \overline{\rho E'' u_i''}\right) - \frac{\partial}{\partial x_i}(\tilde{u}_i\overline{p}) + \overline{\frac{\partial}{\partial x_i}(\tau_{ij}u_j)} + \rho g_i \tilde{u}_i \tag{8.54}$$

The extra terms in Eqs. (8.53) and (8.54) are modeled to solve the compressible turbulent flow equations. The mass-weighted averaged turbulence transport equations for compressible flows are discussed in Appendix I.

8.4 Large eddy simulation (LES)

The idea of LES is developed based on splitting large-scale motions from small scales using a filtering operation such as

$$\overline{\phi}(x) = \int_{\Omega} f(x')G(x, x')dx' \tag{8.55}$$

If the variables of the incompressible Newtonian equations are subjected to the above filtering operation, we get

$$\frac{\partial \overline{u}_i}{\partial x_i} = 0 \tag{8.56}$$

and

$$\frac{\partial \overline{u}_i}{\partial t} + \frac{\partial}{\partial x_j}(\overline{u_i u_j}) = -\frac{1}{\rho}\frac{\partial \overline{p}}{\partial x_i} + \frac{\partial \tau_{ij}}{\partial x_j} + \frac{\partial \tau_{ij}}{\partial x_j}^{SGS} \tag{8.57}$$

where

$$\tau_{ij}^{SGS} = \overline{u}_i\overline{u}_j - \overline{u_i u_j} \tag{8.58}$$

τ^{SGS} in the above equation is generally modeled using various subgrid scale (SGS) models. The standard SGS models [25], dynamic models [26], and nonlinear models are a few to mention. It is a vast area of research and difficult to cover all the theory behind these models in a chapter. For the sake of completeness, we provide the standard SGS model below. The SGS stress of Eq. (8.58) is represented exactly as Eq. (8.13). However, the eddy viscosity is modeled differently here.

8.4.1.1 Standard SGS model

The eddy viscosity here is defined as

$$\nu_T = (C\Delta)^2\bar{\omega} \tag{8.59}$$

The most widely used eddy-viscosity model was proposed by the meteorologist Smagorinsky [25]. Smagorinsky was simulating a two-layer quasi-geostrophic model in order to represent large (synoptic) scale atmospheric motions. He introduced an eddy viscosity that was supposed to model three-dimensional turbulence in the subgrid scales.

In Smagorinsky's model, a mixing-length assumption is made, in which the eddy viscosity is assumed to be proportional to the subgrid scale characteristic length Δ and to a characteristic turbulent velocity based on the second invariant of the filtered field deformation tensor (i.e., strain-rate tensor). In other words, the well-known Smagorinsky's model, where the SGS time scaling, $\bar{\omega}$, in Eq. (8.59) is set as the magnitude of the local resolved strain-rate tensor, namely

$$\bar{\omega} = |\bar{S}| = (2\bar{S}_{ij}\bar{S}_{ij})^{1/2} \tag{8.60}$$

and

$$C = C_s \tag{8.61}$$

If one assumes that the cutoff wave number in Fourier space, $k_c = \pi/\Delta$, lies within a $k^{-5/3}$ Kolmogorov cascade $E(k) = C_K\varepsilon^{2/3}k^{-5/3}$ (where C_K is the Kolmogorov constant), one can adjust the constant C_s so that the ensemble-averaged subgrid kinetic energy dissipation is identical to ε. An approximate value for the constant is

$$C_s \approx \frac{1}{\pi}\left(\frac{3C_K}{2}\right)^{-3/4} \tag{8.62}$$

For a Kolmogorov constant of 1.4, which is obtained by measurements in the atmosphere, this yields, $C_s \approx 0.18$. Most workers prefer $C_s = 0.1$—a value for which Smagorinsky's model behaves reasonably well for free-shear flows and for channel flow. However, the Smagorinsky constant C_s is required to have a sensible value to avoid excessive damping of resolved structures and the grid size Δ, as an indication of characteristic length scale, separates large- and small-scale eddies from each other

and is considered to be an average cell size. It is calculated for three-dimensional elements as follows:

$$\Delta = f(\Delta x_1 \Delta x_2, \Delta x_3)^{1/2} \tag{8.63}$$

Note that the above definition of mesh size can be changed to the usual finite element mesh size as discussed in Chapter 4.

Despite increasing interest in developing more advanced subgrid scale stress models, Smagorinsky's model is still successfully used.

8.5 Detached eddy simulation (DES) and monotonically integrated LES (MILES)

The large eddy simulation (LES), despite less use of empirical relations, needs a very high computational overhead compared to RANS models. This is due to the fact that LES needs a very fine grid in the flow direction to capture flow-aligned streak-like structures occurring in the boundary layers. Motivated by this Spalart et al. [27] suggested an approach that attempts to combine the best features of RANS and LES. This approach is referred to as the detached eddy simulation (DES). This hybrid method reduces to RANS near solid boundaries and LES away from the wall. A minor modification to the SA model presented previously does the trick. Such a model will take advantage of RANS in the thin shear layers close to the walls where RANS models are calibrated. Away from the wall in the separated regions large eddies are resolved.

The model used will be the same as the one in Section 8.2.2 except that the shortest distance to the wall, y, is modified in such a way that the model calculates a RANS eddy viscosity close to the walls and SGS eddy viscosity away from the wall. The modification is simple and given as

$$\tilde{y} = min(y, C_{DES}\Delta) \tag{8.64}$$

Δ has the same meaning as discussed in the previous section. The constant C_{DES} was calibrated for homogeneous turbulence as 0.65. It is now possible to see that close to the walls Δ is larger and the model becomes a RANS model. However, away from the wall the model becomes one for calculating the SGS eddy viscosity [20]. Obviously the difficulty of where and how to fix the grid interface between the RANS and LES zones arises. Two possibilities exist to define this interface. The interface location for the differing models is either explicitly specified, or, based on length scale compatibility, allowed to naturally locate. With the latter approach the location is strongly grid controlled. When explicitly specified (based on turbulence physics grounds), length scale smoothing is necessary to enhance results [28].

The MILES approach [29–31] is similar to LES but instead of using the eddy viscosity, numerical diffusion is used to drain turbulence.

8.6 Direct numerical simulation (DNS)

The direct numerical simulation method can be used to solve all turbulence length scales including the *Kolmogorov* length scale given by Eq. (8.1). The standard Navier-Stokes equation without any modeling is adequate to compute all turbulence scales. The difficulty here is the prohibitively expensive computing cost required to carry out a calculation even at a very small Reynolds number. The enhanced computational overhead is mainly due to the extremely fine mesh necessary to carry out the calculation and the need for higher-order accurate numerical schemes. The number of nodes necessary to resolve all scales in a three-dimensional flow problem may be written in terms of the Reynolds number as (derived based on the assumption that the Kolmogorov length scales are solved)

$$No.Nodes = Re^{9/4} \tag{8.65}$$

Similarly the time step in a calculation is limited by the Kolmogorov time scale in Eq. (8.3). The time step size calculated from the time scale is [32]

$$\Delta t = \frac{0.003H}{u_T\sqrt{(Re_T)}} \tag{8.66}$$

where u_T is the shear velocity and $Re_T = u_T H/2v$ is the turbulence Reynolds number [32].

Although DNS can resolve all turbulence length scales, the currently available computing facilities allow only very small Reynolds number turbulent flow calculations. The turbulence modeling approaches discussed in the previous sections (predominantly RANS) will not be replaced for the foreseeable future.

8.7 Concluding remarks

This chapter was intended to give a brief summary of different turbulence solution techniques. We hope we have summarized all the essential information necessary for a fluid dynamist. The turbulence modeling field is so vast, it may require several books to cover the full details. We recommend the interested reader to refer to the turbulence modeling books listed at the end of this chapter for further details.

References

[1] A.N. Kolmogorov, Local structure of turbulence in incompressible viscous fluid for very large Reynolds number, Doklady Akad. Nauk SSR 30 (1941) 299–303.

[2] B.E. Launder, B. Spalding, Mathematical Models of Turbulence, Academic Press, New York, 1972.

[3] T. Cebeci, A.M.O. Smith, Analysis of Turbulent Boundary Layers, Academic Press, New York, 1974.
[4] D.C. Wilcox, Turbulence Modelling for CFD, DCW Industries Inc., La Canada, CA, 1992.
[5] M. Wolfstein, Some solutions of plane turbulent impinging jets, Trans. ASME J. Basic Eng. 92 (1970) 915–922.
[6] P.R. Spalart, S.R. Allmaras, A one-equation turbulence model for aerodynamic flows, AIAA Paper 92-0439, AIAA 30th Aerospace Sciences Meeting, 1992.
[7] W.P. Jones, B.E. Launder, The prediction of laminarization with a two-equation model of turbulence, Int. J. Heat Mass Transfer 15 (1972) 301–314.
[8] C.K.G. Lam, K. Bremhorst, A modified form of the $\kappa - \varepsilon$ model for predicting wall turbulence, Trans. ASME J. Fluids Eng. 103 (1981) 456–460.
[9] S. Fan, B. Lakshminarayana, M. Barnett, Low-Reynolds-number $\kappa - \varepsilon$ model for unsteady turbulent boundary layer flows, AIAA J. 31 (1993) 1777–1784.
[10] O. Hassan, K. Morgan, J. Peraire, An implicit finite element method for high speed flows, Int. J. Numer. Methods Eng. 32 (1991) 183–205.
[11] K.A. Sorensen, A Multigrid Accelerated Procedure for the Solution of Compressible Fluid Flows on Unstructured Hybrid Meshes, Ph.D. thesis, School of Engineering, University of Wales Swansea, UK, 2001.
[12] E. Fares, W. Schröder, A differential equation for approximate wall distance, Int. J. Numer. Methods Fluids 39 (2002) 743–762.
[13] P.G. Tucker, Differential equation based wall distance computation for DES and RANS, J.Comput. Phys. 190 (2003) 229–248.
[14] C.-B. Liu, P. Nithiarasu, P.G. Tucker, Wall distance calculation using the Eikonal/Hamilton-Jacobi equations on unstructured meshes: A finite element approach, Eng. Comput. 27 (5–6) (2010) 645–657.
[15] P. Nithiarasu, C.-B. Liu, An artificial compressibility based characteristic based split (CBS) scheme for steady and unsteady turbulent incompressible flows, Comput. Methods Appl. Mech. Eng. 195 (2006) 2961–2982.
[16] S.H. Johansson, L. Davidson, E. Olsson, Numerical simulation of vortex shedding past triangular cylinders at high Reynolds number using a $\kappa - \varepsilon$ model, Int. J. Numer. Methods Fluids 16 (1993) 859–878.
[17] P.A. Durbin, Separated flow computations using the $\kappa - \varepsilon - \nu^2$ model, AIAA J. 33 (1995) 659–664.
[18] G. Bosch, W. Rodi, Simulation of vortex shedding past a square cylinder, Int. J. Numer. Methods Fluids 28 (1998) 601–616.
[19] M. Tutar, A.E. Holdo, Computational modelling of flow around a circular cylinder in sub-critical flow regime with various turbulence models, Int. J. Numer. Methods Fluids 35 (2001) 763–784.
[20] G. Constantinescu, C. Matthieu, K. Squires, Turbulence modelling applied to flow over a sphere, AIAA J. 41 (2003) 1733–1742.
[21] J. Laufer, Investigation of turbulent flow in a two-dimensional channel, NACA Rep. 1053 (1951) 1247–1266.

[22] M.K. Denham, P. Briard, M.A. Patrick, A directionally-sensitive laser anemometer for velocity measurements in highly turbulent flows, J. Phys. E: Sci. Instrum. 8 (1975) 681–683.
[23] Z. Yang, T.H. Shih, New time scale based $\kappa - \varepsilon$ model for near-wall turbulence, AIAA J. 31 (1993) 1191–1198.
[24] H. Schlichting, Boundary Layer Theory, Pergamon Press, London, 1955.
[25] J. Smagorinsky, General circulation experiments with the primitive equations. I. The basic experiment, Mon. Weather Rev. 91 (1963) 99.
[26] M. Germano, Turbulence: the filtering approach, J. Fluid Mech. 238 (1992) 325.
[27] P.R. Spalart, W.H. Jou, M. Strelets, S.R. Allmaras, Comments on the feasibility of LES for wings, and on a hybrid RANS/LES approach, in: C. Liu, Z. Liu (Eds.), Advances in DNS/LES: First AFOSR International Conference on DNS/LES, Greyden, Columbus, OH, 1997.
[28] P.G. Tucker, L. Davidson, Zonal k-1 based large eddy simulations, Comput. Fluids 33 (2004) 267–287.
[29] J.P. Boris, F.F. Grinstein, E.S. Oran, R.L. Kolbe, New insights into large eddy simulation, Fluid Dyn. Res. 10 (1992) 199–228.
[30] P.G. Tucker, Novel MILES computations for jet flows and noise, Int. J. Heat Fluid Flow 25 (2004) 625–635.
[31] W.J. Rider, Effective subgrid modeling from the ILES simulation of compressible turbulence, J. Fluids Eng. 129 (2007) 1493–1496.
[32] J. Kim, P. Moin, R. Moser, Turbulence statistics in fully developed channel flow at low Reynolds numbers, J. Fluid Mech. 177 (1987) 133–166.